Observation of a hierarchy of up to fifth-order rogue waves in a water tank

A. Chabchoub,[1,*] N. Hoffmann,[1] M. Onorato,[2,3] A. Slunyaev,[4] A. Sergeeva,[4] E. Pelinovsky,[4] and N. Akhmediev[5]

[1]*Mechanics and Ocean Engineering, Hamburg University of Technology, Eißendorfer Straße 42, 21073 Hamburg, Germany*

[2]*Dipartimento di Fisica, Università degli Studi di Torino, Torino 10125, Italy*

[3]*Istituto Nazionale di Fisica Nucleare, INFN, Sezione di Torino, 10125 Torino, Italy*

[4]*Department of Nonlinear Geophysical Processes, Institute of Applied Physics, Nizhny Novgorod, Russia*

[5]*Optical Sciences Group, Research School of Physics and Engineering, The Australian National University, Canberra, ACT 0200, Australia*

(Received 19 July 2012; published 6 November 2012)

We present experimental observations of the hierarchy of rational breather solutions of the nonlinear Schrödinger equation (NLS) generated in a water wave tank. First, five breathers of the infinite hierarchy have been successfully generated, thus confirming the theoretical predictions of their existence. Breathers of orders higher than five appeared to be unstable relative to the wave-breaking effect of water waves. Due to the strong influence of the wave breaking and relatively small carrier steepness values of the experiment these results for the higher-order solutions do not directly explain the formation of giant oceanic rogue waves. However, our results are important in understanding the dynamics of rogue water waves and may initiate similar experiments in other nonlinear dispersive media such as fiber optics and plasma physics, where the wave propagation is governed by the NLS.

DOI: 10.1103/PhysRevE.86.056601 PACS number(s): 05.45.Yv, 47.20.Ky, 42.65.−k, 92.10.Hm

I. INTRODUCTION

The nonlinear Schrödinger equation (NLS) describes a variety of nonlinear wave processes in physics, including gravity waves on the surface of the deep ocean [1,2]. It has been well established that the NLS has a hierarchy of rational solutions that describe doubly localized structures with infinitely increasing amplitude as its order increases [3–7]. The lowest-order structure of this hierarchy is known as the Peregrine breather [8]. Due to its localization both in time and in space it is considered to be a prototype of a rogue wave in the ocean [9] that has the remarkable property to "appear from nowhere and disappear without a trace" [10]. All higher-order structures of this family have the same property and in addition have progressively increasing amplitudes [11]. As such, they would describe rogue waves of significantly higher ratio of peak to the background amplitude.

Theoretically, expressions for these solutions can be written in general form for any order [4–7,12]. However, explicit formulas become cumbersome with increasing order, and the highest order to which a solution is presently known is eight [13]. Difficulties in writing the solution are reoccurring when they are observed experimentally. The Peregrine breather has been observed recently in optics [14], in a water wave tank [15], and in plasma [16]. The second-order structure, or "superrogue wave," has also been observed in the case of deep-water waves [17]. Thus, fundamentally, the existence of two lowest-order structures in experiment has been proven. However, the higher-order structures of this hierarchy still have to be shown to exist. This is not an easy task as these waves, in addition to high amplitude, have higher steepness. In order to keep the parameters of the structure within the allowed limitations, one has to choose carefully the initial conditions for their excitation.

In this work, we are able to demonstrate the existence of higher-order rational solutions on a water surface up to fifth order. This seems to be the maximum order which we can achieve, at least with our existing experimental equipment. This is a remarkable achievement taking into account the approximate nature of modeling deep-water waves with the NLS. Of course, we are far from claiming that these solutions can describe real oceanic rogue waves [1,18–22]. However, our results show clearly that nonlinearity may play a central role in the dynamics of water waves. As such, these results can be considered as significant progress in our understanding of water wave dynamics.

II. THEORETICAL BACKGROUND

The NLS is one of the fundamental equations in theoretical physics. Generally, it describes one-dimensional evolution in time and space of weakly nonlinear wave packets in optics, hydrodynamics, and plasmas and, more generally, in nonlinear dispersive media [23,24]. In particular, it describes the propagation of deep-water waves [25–27]. For this purpose, the NLS can be written as

$$i\left(\frac{\partial A}{\partial t}+c_g\frac{\partial A}{\partial x}\right)-\frac{\omega_0}{8k_0^2}\frac{\partial^2 A}{\partial x^2}-\frac{\omega_0 k_0^2}{2}|A|^2A=0, \quad (1)$$

where x and t are the spatial and time coordinates, respectively, and ω_0 and k_0 denote the wave frequency and the wave number of the carrier wave. The dispersion relation of linear deep-water wave trains is given by $\omega_0=\sqrt{gk_0}$, where g is the gravitational acceleration. The wave group velocity is $c_g:=\frac{d\omega}{dk}|_{k=k_0}=\frac{\omega_0}{2k_0}$. The surface elevation of water waves $\eta(x,t)$ can be calculated from the NLS variable $A(x,t)$. To second order in steepness it is given by

$$\eta(x,t)=\mathrm{Re}\{A(x,t)\exp[i(k_0x-\omega_0t)]\}+\mathrm{Re}\left\{\tfrac{1}{2}k_0A^2(x,t)\exp[2i(k_0x-\omega_0t)]\right\}. \quad (2)$$

*amin.chabchoub@tuhh.de

When dealing with exact solutions, it is convenient to use the dimensionless form of the NLS,

$$i\psi_T + \psi_{XX} + 2|\psi|^2\psi = 0, \tag{3}$$

which is obtained from Eq. (1) using the rescaled variables:

$$T = -\frac{\omega_0}{8}t, \quad X = (x - c_g t)k_0 = xk_0 - \frac{\omega_0}{2}t, \quad \psi = \sqrt{2}k_0 A. \tag{4}$$

Here, X is the coordinate in a frame moving with the group velocity, and T is the rescaled time.

Generally, the NLS has a hierarchy of breather solutions localized in space and time [3,8,10]. They pulsate only once, thus representing a class of solutions that can be considered a model for oceanic rogue waves. The j-order rational solution of the NLS in general form, also known as the jth Akhmediev-Peregrine solution, can be written in the form

$$\psi_j(X,T) = \psi_0\left[(-1)^j + \frac{G_j + iH_j}{D_j}\right]\exp(2i|\psi_0|^2 T), \tag{5}$$

where the background amplitude is ψ_0 and the polynomials $G_j(X,T)$, $H_j(X,T)$, and $D_j(X,T)$ can be found in Ref. [11] for a few lowest-order solutions. In particular, for the Peregrine breather, $G_1 = 4$, $H_1 = 16|\psi_0|^2 T$, and $D_1 = 1 + 4|\psi_0|^2 X^2 + 16|\psi_0|^4 T^2$. The corresponding expressions for higher-order solutions are progressively more complicated. To give an example, the expressions for the eighth-order solution written similarly would require 60 printed pages [13]. We assume that the polynomials G_j, H_j, and D_j for $j = 3,4,5$ are known from Refs. [3,5,6] and will not copy them here. The amplitude profiles for rational solutions up to fourth order are illustrated in Fig. 1. The central amplitude is equal to $(2j+1)\psi_0$. It increases progressively with j.

Experimental explorations of this class of breather solutions started recently with the Peregrine breather, observed first in fiber optics [14], in a water tank [15], and in plasma [16]. The second-order solution was observed only in the case of water waves [17]. In the present work, we took further steps in order to observe third-, fourth-, and fifth-order solutions in a water wave tank.

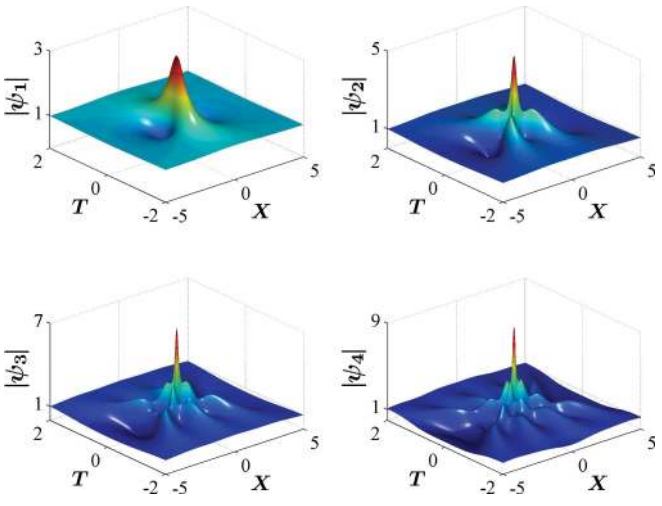

FIG. 1. (Color online) Higher-order Akhmediev-Peregrine rational solutions of the NLS with the background amplitude $\psi_0 = 1$. At $X = 0$ and $T = 0$ the maximal amplitude amplification of the jth solution is $2j + 1$.

III. OBSERVATIONS OF THE HIGHER-ORDER ROGUE WAVES

The present experiments were conducted in a 15 m × 1.6 m × 1.5 m water wave tank. An illustration and technical details of the tank can be found in Ref. [15]. The single-flap wave maker is computer controlled to generate the desired wave shapes and heights. To avoid wave reflections, an absorbing beach is installed at the opposite end. All experiments are conducted in deep-water conditions, with the ratio of the water depth h of 1 m to the wavelength being much larger than unity. The water surface elevation at any given point is measured by a capacitance wave gauge with a sensitivity of 1.06 V/cm and a sampling frequency of 0.5 kHz, placed at a distance 9 m from the flap.

In order to generate rational breathers representing giant rogue waves in the tank, one has to fix the initial amplitude a_0 and the steepness $\varepsilon = a_0 k_0$ of the carrier wave. Once the amplitude and the steepness are determined, it is straightforward to find the wave number k_0 and to derive the wave frequency from the linear dispersion relation, i.e., $\omega_0 = \sqrt{gk_0} = \sqrt{\frac{g\varepsilon}{a_0}}$. Then, using the relation $\psi_0 = a_0\sqrt{2}k_0$ and inverting the scaling in Eq. (4), the analytical solution can be converted to dimensional form.

To determine the boundary conditions for the wave maker, the dimensionalized analytical solution of the NLS (5) is translated along the tank in order to observe the position of maximal amplitude of the rational solutions ($x = 0$) closer to the beach. Then the expression for the surface elevation, Eq. (2), is used to calculate the initial condition at the position of the paddle, which is $x = -9$ m. Such an arrangement produces the maximal amplitude of the breather at a distance of 9 m from the flap.

In order to calibrate our wave-generating equipment, first, we measured the response function of the flap. Namely, we generated a pure sinusoidal wave with a given amplitude at the output of the computer signal controlling the flap and measured the water wave amplitude in the tank. The plot of water wave amplitude versus the amplitude of the computer signal is shown in Fig. 2. It can be seen that within the range of amplitudes we are dealing with, this plot is linear. The corresponding coefficient of this linear response function has been used in the computer program in further experiments.

The first observation of a Peregrine soliton evolution in water waves was reported in Ref. [15]. It was done at a fixed frequency $\omega_0 = 10.68\ \mathrm{s}^{-1}$, an amplitude of $a_0 = 0.01$ m, and a water depth value of $h = 1$ m in the tank. In order to confirm that the Peregrine breather does exist for a wider range of parameters of the experimental setup, we repeated these observations. Figure 3 shows another example of a measured Peregrine breather. Here, the steepness of the carrier is $\varepsilon = 0.09$, and the background wave has an elevation amplitude of 0.5 cm. Therefore, the frequency is $\omega_0 = 13.29\ \mathrm{s}^{-1}$. Then, the maximal amplitude amplification is 3, providing an amplitude of the rogue wave of 1.5 cm.

The first experimental demonstration of the second-order Akhmediev-Peregrine soliton was reported earlier in Ref. [17].

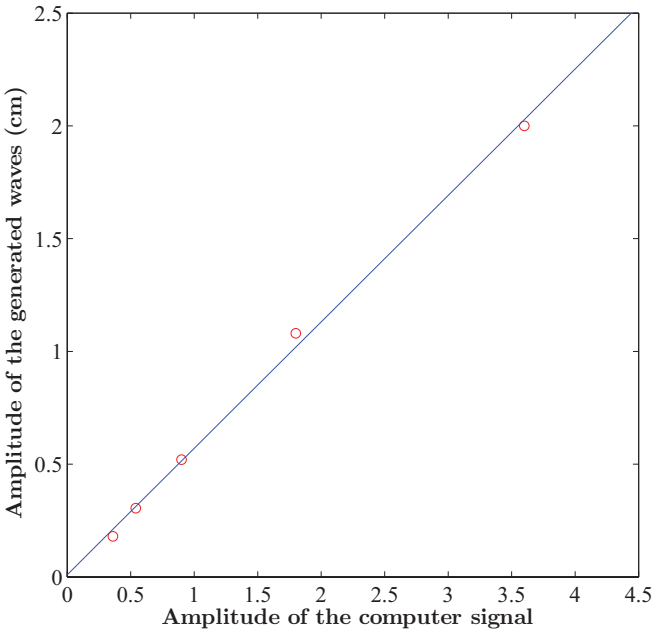

FIG. 2. (Color online) Response function of the flap for a fixed steepness value $\varepsilon = 0.1$ and a fixed depth $h = 1$ m.

Figure 4 shows another observation for the parameter values of $a_0 = 3$ mm and $k_0 = 13.33$ m^{-1}; hence, $\omega_0 = 11.43$ s^{-1}. As predicted in theory, the carrier wave reaches its maximal amplitude amplification of 5 at the center of the breather. Generally, in order to generate higher-order breather solutions in a water wave tank, the carrier parameters have to be carefully chosen to avoid significant distortions related to wave breaking. As the local steepness of the wave in this case is higher than for the Peregrine breather, we have to reduce carrier steepness to 0.04 and its amplitude to 3 mm. Thus, the maximum amplitude of the second-order breather reaches 15 mm.

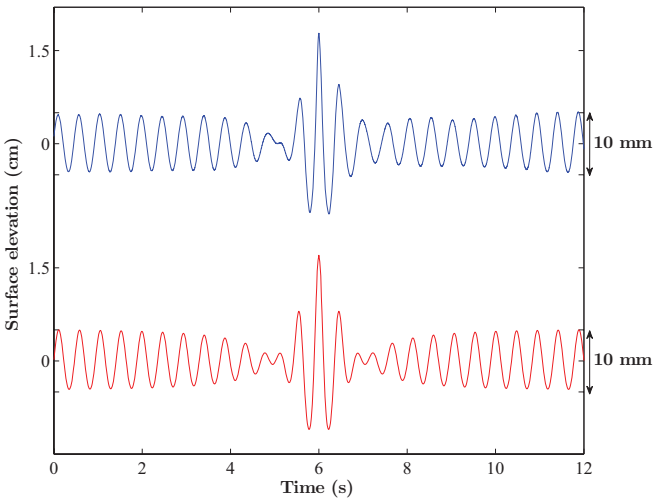

FIG. 3. (Color online) Experimental observation of the Peregrine soliton at $x = 0$ for carrier parameters $a_0 = 5$ mm and $\varepsilon = 0.09$ (blue top curve). For comparison, the theoretical prediction at the same position is shown by the red bottom curve.

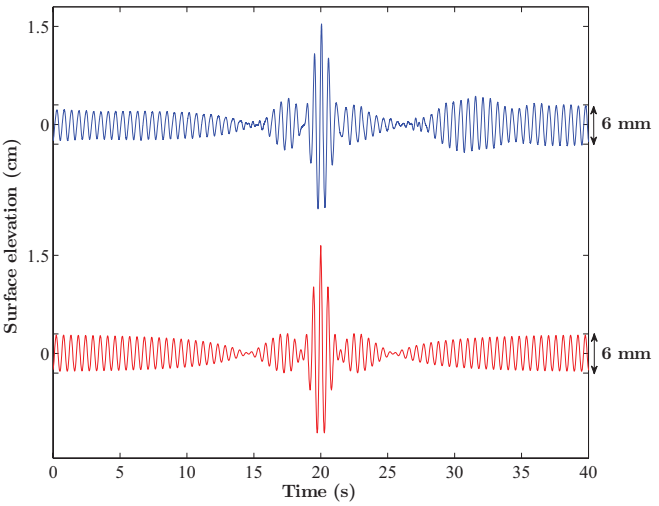

FIG. 4. (Color online) Experimental demonstration of the second-order rational breather at $x = 0$ for carrier wave parameters $a_0 = 3$ mm and $\varepsilon = 0.04$ (blue top curve). For comparison, the theoretical curve at the same spatial position is shown by the red bottom curve.

Figure 5 presents experimental demonstrations of the third-order breather solution. These are observed for several steepness values of the background wave, namely, 0.04 [Fig. 5(a)], 0.03 [Fig. 5(b)], and 0.02 [Fig. 5(c)], and carrier amplitudes of 0.05 cm [Fig. 5(a)], 0.1 cm [Fig. 5(b)], and 0.2 cm [Fig. 5(c)], respectively. For these amplitudes, experimental curves are reasonably well described by the theory with an amplification factor of 7 being reached at the peak of the breather for all three cases. Relatively small background amplitudes are crucial for these observations. The curves are becoming asymmetric when the background steepness increases, as can be seen from Fig. 5(c). The presence of such an asymmetry when increasing the carrier steepness was also observed for the Peregrine solution in Ref. [28] and for the second-order solution in

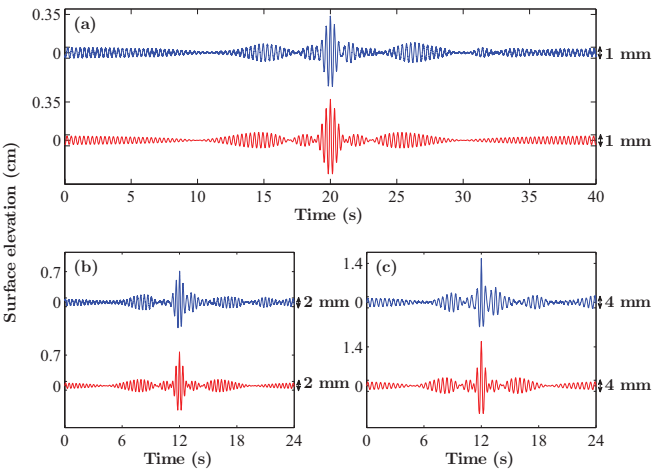

FIG. 5. (Color online) Three experimental observations (blue top curves) of the third-order rational breather at $x = 0$ for carrier wave parameters (a) $a_0 = 2$ mm and $\varepsilon = 0.04$, (b) $a_0 = 1$ mm and $\varepsilon = 0.03$, and (c) $a_0 = 0.5$ mm and $\varepsilon = 0.02$. For comparison, the theoretical predictions at the same positions are shown by the red bottom curves.

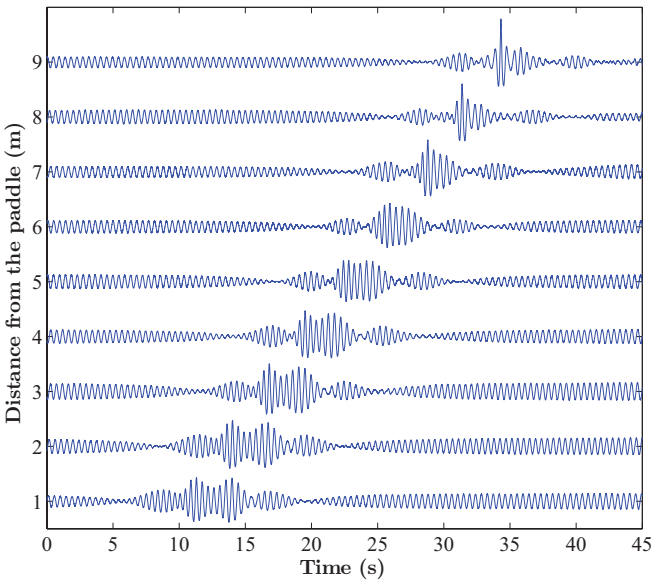

FIG. 6. (Color online) Evolution of the third-order rogue wave along the water wave tank for carrier parameters $a_0 = 2$ mm and $\varepsilon = 0.04$. The curves are measured at distances separated by 1 m from each other.

Ref. [17]. A further increase of the background steepness results in a breaking of the wave near the center of the breather.

Figure 6 shows the spatial evolution of the third-order rational solution along the tank. The lowest curve is measured at a distance of 1 m from the starting end of the tank; i.e., it is close to the paddle. The upper curve is measured at a distance of 9 m from the paddle, i.e., at the location of the maximum amplitude of the breather. The intermediate curves, taken at distances separated by 1 m from each other, show the growth of the central amplitude of the third-order breather and the concentration of wave energy towards the central area of the breather at the developed stage of evolution. They also show that the whole localized formation moves with the group velocity. The limited length of the tank does not allow us to observe the complete evolution of the breather starting from slightly perturbed sinusoidal wave. The distance required for half of the evolution length until the maximum is reached can be estimated as around 100 m. Thus, we had to start with the initial condition at $x = -9$ m when the perturbation grew noticeably. This would be the limitation for most of the water tanks used in laboratories.

Figure 7 presents experimental observations of the fourth-order breather solution. These experiments are done for background amplitudes of 1 and 3 mm for steepness values of 0.02 and 0.03, respectively. The expected wave amplitude amplification factor of 9 is reached in these experiments remarkably well. Unavoidable asymmetry of the curves appears when increasing the steepness of the carrier.

The highest-order breather that we were able to observe so far is the fifth-order solution. These results are shown in Fig. 8. The theoretical amplification factor of the carrier amplitude here is 11, which is a remarkable fact by itself, despite the background wave amplitude being only 1 mm. Any attempts to generate sixth- and higher-order breathers failed as the wave breaking ruined the central part of the breather, thus reducing

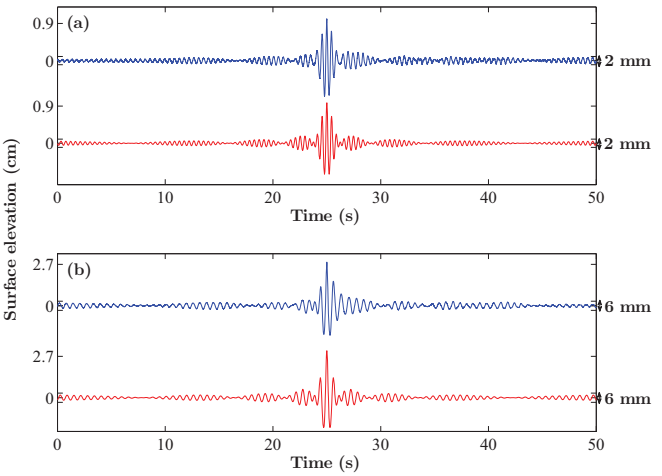

FIG. 7. (Color online) Two observations of the fourth-order rational breather at $x = 0$ for carrier parameters (a) $a_0 = 1$ mm and $\varepsilon = 0.02$ in and (b) $a_0 = 3$ mm and $\varepsilon = 0.03$ (blue top curves) compared to the theoretical prediction at the same position (red bottom curves).

the central peak significantly. As a result, the whole wave evolution has been greatly distorted.

IV. EXPERIMENTAL LIMITATIONS AND BREAKING LIMITS

There are a few restrictions that have to be mentioned related to the experimental observations described above. Higher-order solutions have a multipeak structure and increased derivative relative to the first-order solution. Taking this into account is essential when setting up higher-order solutions. First, the spatial extension of the higher-order breathers increases strongly with the order. The higher the order of the breather is, the longer the space needed for the

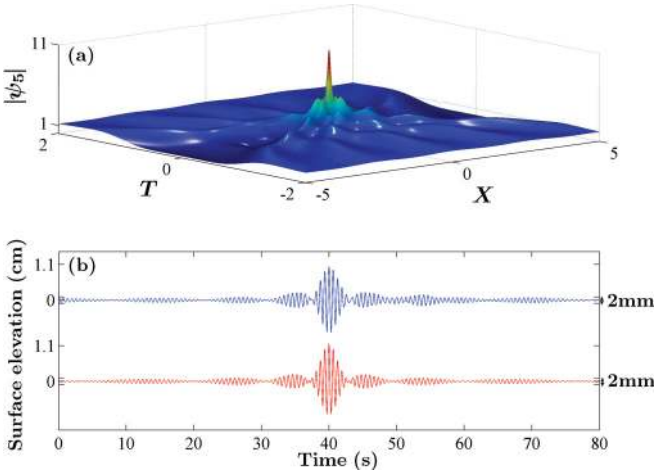

FIG. 8. (Color online) (a) Fifth-order Akhmediev-Peregrine rational solutions of the NLS with the background $\psi_0 = 1$. (b) Observations of the fifth-order rational breather at $x = 0$ for carrier wave parameters $a_0 = 1$ mm and $\varepsilon = 0.01$ (blue top curve) compared to the theoretical prediction at the same position (red bottom curve).

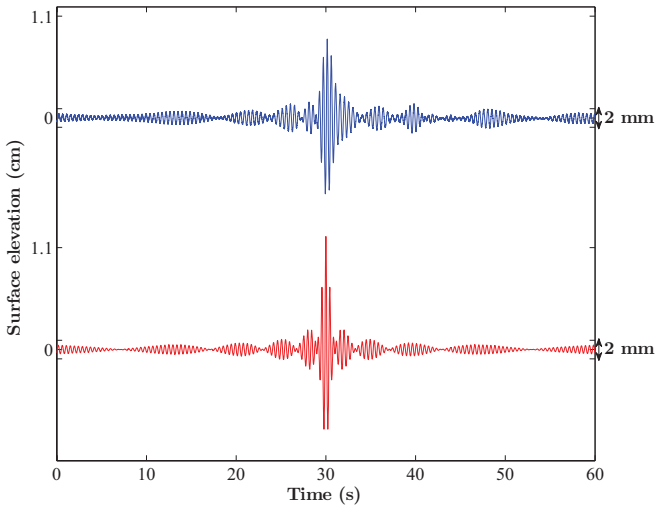

FIG. 9. (Color online) Measurement of the fifth-order rational breather which breaks before reaching the maximal amplitude amplification at $x = 0$ for carrier parameters $a_0 = 1$ mm and $\varepsilon = 0.02$ (blue top curve) compared to the theoretical prediction at the same position (red bottom curve).

breather to develop is; therefore, due to the limited size of the tank, the higher order must be the initial wave amplitude generated by the flap. For example, for the fifth-order solution, in order to observe the solution at a distance 9 m from the flap, the initial amplitude of the wave after the flap has to be as high as about 10 times the amplitude of the underlying carrier Stokes wave. Thus, the tank length provides a relatively small part of the breather evolution. However, 9 m in the experiment still correspond to 14 wavelengths, and we can clearly observe the nonlinear evolution of the most essential central part of the breather.

Second, significant local amplification of the wave amplitude of the breather means that the wave breaking may occur before the highest amplitude is reached. Indeed, Fig. 9 shows that due to the breaking of the wave, the amplitude amplification of 11 expected for the fifth-order solution is not reached. This happens when the carrier steepness is increased to 0.02, while the amplitude is 1 mm, i.e., the same as in Fig. 8(b). Since the objective of the present study is to generate higher-order solutions with the best possible accuracy, we tried to keep the amplitudes at sufficiently low level. Thus, very low steepness values of the carrier wave have been used. We avoided exceeding criteria for local breaking during the whole wave evolution. Controlling the steepness for each breather, we found that spilling type breaking occurs for the experimentally estimated threshold carrier steepness values ε_b shown in Table I.

Keeping the steepness values low did not allow us to reach high amplitudes for breathers in absolute terms. Nevertheless, the ratio of the peak amplitude to the background amplitude was confirmed to agree with the theory. The latter increases with the order of the solution. We should note that the wave breaking is a process independent from breather generation. The distance at which the breaking of an initially sinusoidal wave occurs depends on the amplitude of this wave and generally decreases with the amplitude.

TABLE I. Lowest threshold carrier wave steepness value for each rational breather when wave breaking starts.

Rational solutions	Threshold steepness value ε_b
First order	0.12
Second order	0.06
Third order	0.05
Fourth order	0.04
Fifth order	0.02

V. SUMMARY

We have confirmed, experimentally, that the higher-order rational breather solutions of the NLS can be generated in conditions of deep-water gravity waves. Up to fifth order a breather can be observed in a 15 m tank without being significantly distorted by the wave-breaking effect and the limitations of the short tank.

The steepness of the carrier wave is the crucial parameter in these observations. The smaller the carrier steepness is, the better the agreement is with the theoretical NLS prediction. For each observed rational breather we determined the carrier steepness values when the corresponding amplified wave starts to break. Due to this limitation, the absolute values of peak amplitudes for higher-order solutions cannot be significantly increased. However, the ratio of peak amplitude to the background wave increases in accordance with the theory.

Clearly, the results of experimental observation of higher-order breathers in the water tank cannot be directly applied to explain giant ocean rogue waves. First, the probability of their excitation in a chaotic wave field would be extremely low. Second, wave-breaking phenomena would destroy them well before they reached high amplitudes. Third, the steepness values of our experiment are significantly smaller than steepness values related to the ocean. Furthermore, there are myriad other factors that differ between the ocean and an ideal laboratory setup. Nevertheless, the mere fact that such solutions can be observed proves the validity of the nonlinear approach to the dynamics of water waves. It also shows that the range of phenomena described by the NLS is significantly richer than the simple world of solitons and small-amplitude radiation waves. This world is not complete if we do not take into account the whole hierarchy of breathers.

ACKNOWLEDGMENTS

A.C. would like to thank Pierre Gaillard for helpful discussions. N.H., E.P., A.Se. and N.A. acknowledge the support of the Volkswagen Stiftung. N.A. acknowledges partial support of the Australian Research Council (Discovery Project No. DP110102068). E.P. acknowledges support from RFBR grant 11-05-00216, A.Sl. acknowledges support from RFBR grant 11-02-00483, and A.Se. is supported by the President's grant MK-4378.2011.5. M.O. was supported by ONR grant N000141010991 and by the European Union under the project EXTREME SEAS (SCP8-GA-2009-234175). N.A. acknowledges support from the Alexander von Humboldt Foundation.

[1] A. Osborne, *Nonlinear Ocean Waves and the Inverse Scattering Transform* (Elsevier, Amsterdam, 2010).
[2] M. J. Lighthill, J. Inst. Math. Appl. **1**, 269 (1965).
[3] N. Akhmediev, V. M. Eleonskii, and N. E. Kulagin, Zh. Eksp. Teor. Fiz. **89**, 1542 (1985) [Sov. Phys. JETP **61**, 894 (1985)].
[4] P. Dubard and V. B. Matveev, Nat. Hazards Earth Syst. Sci. **11**, 667 (2011).
[5] P. Gaillard, Sci. Adv. **13**, 71 (2012).
[6] P. Gaillard (unpublished), http://hal.archives-ouvertes.fr/hal-00650528.
[7] Y. Ohta and J. Yang, Proc. R. Soc. A **468**, 1716 (2012).
[8] D. H. Peregrine, J. Aust. Math. Soc., Ser. B **25**, 16 (1983).
[9] V. I. Shrira and V. V. Geogjaev, J. Eng. Math. **67**, 11 (2010).
[10] N. Akhmediev, A. Ankiewicz, and M. Taki, Phys. Lett. A **373**, 675 (2009).
[11] N. Akhmediev, A. Ankiewicz, and J. M. Soto-Crespo, Phys. Rev. E **80**, 026601 (2009).
[12] P. Dubard, P. Gaillard, C. Klein, and V. Matveev, Eur. Phys. J. Spec. Top. **185**, 247 (2010).
[13] P. Gaillard (unpublished), http://hal.archives-ouvertes.fr/hal-00664052.
[14] B. Kibler, J. Fatome, C. Finot, G. Millot, F. Dias, G. Genty, N. Akhmediev, and J. M. Dudley, Nat. Phys. **6**, 790 (2010).
[15] A. Chabchoub, N. P. Hoffmann, and N. Akhmediev, Phys. Rev. Lett. **106**, 204502 (2011).
[16] H. Bailung, S. K. Sharma, and Y. Nakamura, Phys. Rev. Lett. **107**, 255005 (2011).
[17] A. Chabchoub, N. Hoffmann, M. Onorato, and N. Akhmediev, Phys. Rev. X **2**, 011015 (2012).
[18] L. Draper, Mar. Obs. **35**, 193 (1965).
[19] R. G. Dean, in *Water Wave Kinematics*, edited by A. Torum and O. T. Gudmestad (Kluwer, Dordrecht, 1990), pp. 609–612.
[20] P. Müller, C. Garrett, and A. Osborne, Oceanography **18**, 66 (2005).
[21] S. Perkins, Sci. News **170**, 328 (2006).
[22] C. Kharif, E. Pelinovsky, and A. Slunyaev, *Rogue Waves in the Ocean* (Springer, Heidelberg, 2009).
[23] R. Y. Chiao, E. Garmire, and C. H. Towns, Phys. Rev. Lett. **13**, 479 (1964).
[24] D. J. Benney and A. C. Newell, J. Math. Phys. **46**, 133 (1967).
[25] V. E. Zakharov, J. Appl. Mech. Tech. Phys. **9**, 190 (1968).
[26] H. C. Yuen and B. M. Lake, Adv. Appl. Mech. **22**, 67 (1982).
[27] H. C. Yuen and B. M. Lake, Phys. Fluids **18**, 956 (1975).
[28] A. Chabchoub, N. Akhmediev, and N. P. Hoffmann, Phys. Rev. E **86**, 016311 (2012).